Effect of microstructure heterogeneity on the damage resistance of nacre-like alumina: insights from image-based discrete simulations

Kaoutar Radi, Hassan Saad, David Jauffrès, Sylvain Meille, Thierry Douillard, Sylvain Deville, Christophe L. Martin

Effect of microstructure heterogeneity on the damage resistance of nacre-like alumina: insights from image-based discrete simulations

Kaoutar Radi[a], Hassan Saad[b,c], David Jauffres[a,*], Sylvain Meille[b], Thierry Douillard[b], Sylvain Deville[c,d], Christophe L. Martin[a]

[a] *Univ. Grenoble Alpes, CNRS, Grenoble INP, SIMaP, Grenoble, France*
[b] *Université de Lyon, INSA Lyon, MATEIS CNRS UMR5510, Villeurbanne, France*
[c] *Laboratoire de Synthèse & Fonctionnalisation des Céramiques, UMR3080 CNRS-Saint-Gobain, 84306 Cavaillon, France*
[d] *now with: Université de Lyon, Université Claude Bernard Lyon1, CNRS, Institut Lumière Matière, 69622 Villeurbanne, France*

Abstract

Recently, several types of nacre-like materials have been developed using various methods. However, the resulting materials exhibit a significant randomness and defects compared to natural nacre. Therefore, evaluating the influence of these microstructural variations on the material's mechanical behavior is of high interest for the development of nacre-like materials and their industrial scale-up. In this work, we present an original method that allows the modeling of complex morphology of brick and mortar materials, by combining Discrete Element Method and Electron Backscatter Diffraction images. Using different realistic microstructures we studied the effect of the microstructural variations on crack propagation and damage resistance. The obtained results were compared to the regular microstructure of nacre and showed a non-negligible decrease of mechanical properties.

Keywords: Ceramics, toughness, DEM, nacre, EBSD

Owing to its unique microstructure, nacre, the inner part of some seashells, presents a toughness several orders of magnitude larger than that of its constituents. Using different fabrication techniques, scientists succeeded in developing bioinspired brick-and-mortar nacre-like materials, either with a ductile [1, 2, 3, 4] or a brittle interface [5, 6, 7], that provide promising mechanical properties. However, the resulting microstructures, that mimic the brick and mortar architecture of natural nacre, are not as perfect as those produced by seashells and exhibit a significant randomness and defects compared to natural nacre. Well-aligned periodic materials can be produced only at larger constituent length scales using either manual assembly [8], 3D printing [9] or laser engraving [10]. Reproducing the actual length scale of the biomaterial microstructure is nonetheless a key point to maximize the bioinspired material performance [11, 12, 13]. Assessing the influence of hardly avoidable microstructural variations and alignment defects on mechanical behavior is thus of high interest for the development of nacre-like materials and their industrial scale-up.

Most of the modeling studies conducted on nacre-like materials showed that introducing microstructural variations degrades both strength [15] and toughness [16]. Nevertheless, it has been shown that in some configurations, microstructural variations are beneficial. For example, in ductile crack growth, a non-uniform distribution of obstacles leads to higher toughness than when obstacles are equally distributed [17]. For nacre-

*Corresponding author
Email address: david.jauffres@grenoble-inp.fr (David Jauffres)

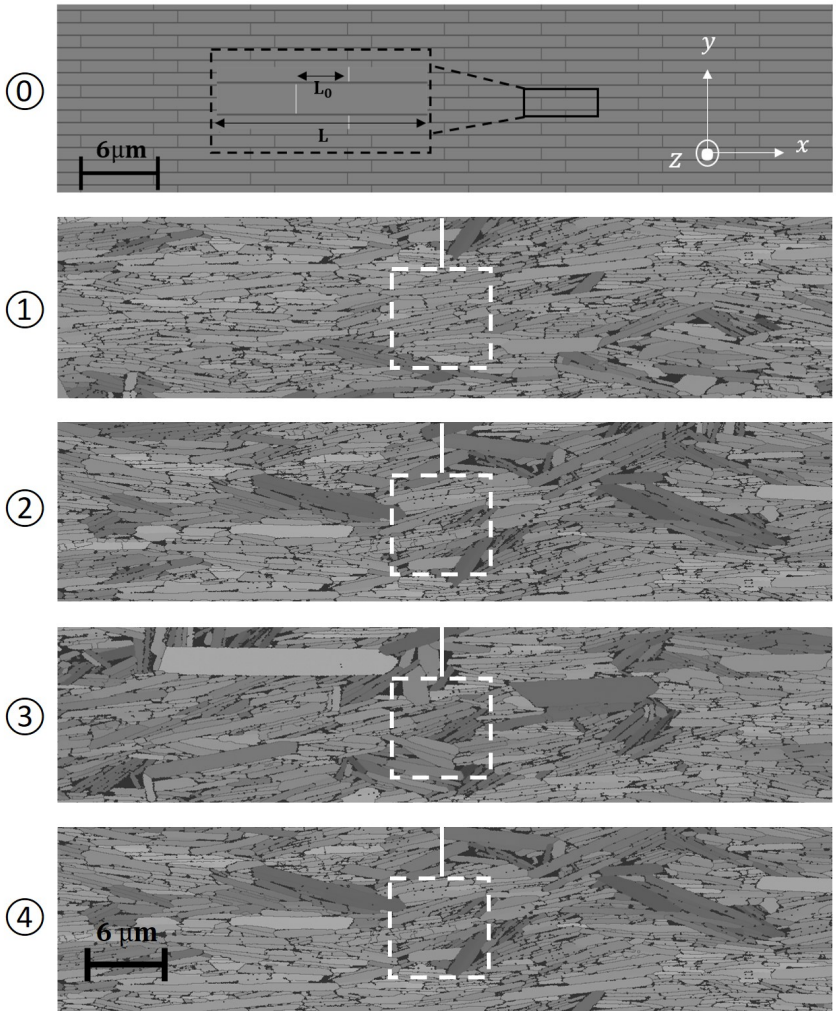

Fig. 1: The five microstructures used in our simulations a) The regular brick and mortar microstructure (M0) used in [14] and a close-up of the overlap region. b) Index quality map resulting from EBSD analysis of a nacre-like alumina sample showing the four images (1-4) that were used in DEM simulations to generate four notched numerical microstructures M1-M4. The dashed white squares highlight the zones ahead of the crack tip used to compute the local microstructure parameters reported in Tab. 2.

like materials, a recent study also suggests that some random variations in the microstructure can improve toughness [18]. All prior modeling studies on the effect of microstructural variations were focused on materials with ductile interfaces and the microstructural variations considered were only the introduction of dispersion on the main microstructural parameters characterizing the regular structure. Also, most of those studies consider that the tablets are rigid, a questionable hypothesis in the case of low tablet/interface Young's moduli contrast [14, 6]. Here, we present an original method that allows modeling more realistic morphology of brick and mortar materials, by combining Discrete Element Method (DEM) and Scanning Electron Microscopy (SEM) images from Electron Backscatter Diffraction (EBSD) analysis. We investigate the effect of microstructural variations on crack propagation and damage resistance by analyzing the numerical mechanical response of four different realistic microstructures obtained by compaction and field-assisted sintering (FAST) as compared to a regular, numerically generated, microstructure.

To model crack propagation using realistic microstructures of nacre-like alumina, we combine microscopy images originating from EBSD analysis with numerical DEM simulations. The DEM

formulation and the sample generation procedure are similar to our earlier study on a Representative Volume Element (RVE)[19]. To model the mechanical behavior of continuous media with DEM, we consider the material as a random packing of spherical particles bonded by cylindrical beams that obey elastic interaction laws together with Rankine fracture criteria [20, 19]. After an individual calibration procedure of the interaction laws for each constituent (tablet and interface) the model has been successfully confronted to existing analytical shear-lag models at the scale of a single RVE [19]. As compared to analytical models or finite element models the present approach allows fracture and damage processes within both the interfaces and the tablets to be easily accounted for by the fracture criteria at the scale of the DEM bond. Recently, the approach was extended to study crack propagation within a nacre-like microstructure at a larger scale (about a hundred tablets)[14]. A typical packing contains about 1 million particles, the number of particles was chosen to get at least three particles per interface to ensure results convergence [19].

Once a random packing of particles has been generated, the second step is the image preparation. The images used are shown in Fig.1. M0 (Fig.1a) is a regular microstructure numerically generated [14], where tablets and interface are perfectly aligned with a constant tablet aspect ratio and interface thickness. The overlap ratio (overlap length L_0/ tablet length L) is set to 0.25 i.e. the mean value expected for a random distribution of overlaps [14]. Images 1 to 4 are from the EBSD analysis of a nacre-like alumina sample (Fig.1b). The sample was obtained by Field Assisted Sintering Technique (FAST) with uniaxial pressure [6]. The initial powder is composed of anisotropic alumina platelets, alumina nanoparticles and glass-phase precursors ($CaCO_3$, SiO_2) [5]. During FAST treatment, the liquid glass assists the sintering and forms with alumina nanoparticles the "mortar" between tablets. The relative density of the material is 98 % [6]. The EBSD acquisition was performed using an Oxford Instruments detector installed on a Zeiss Supra 5S SEM microscope with a step size of 80 nm for the analysis. In this work we use the index quality map (Fig.1b) that displays an excellent contrast between crystalline lamellae with a good indexing quality (white to light gray) and the amorphous interface material that cannot be indexed (black). The images are binarized and used as a mask on the discrete packings. For each particle in the packing, the color of the voxel geometrically corresponding to the particle center defines the material type: tablet or interface. The contact law parameters are then calibrated to reproduce the mechanical behavior of each phase [20, 21].

In order to assess the crack extension resistance (R-curve) of the microstructures, a Single Edge Notch Tensile (SENT) configuration was used. A notch is introduced in all samples and quasistatic tensile tests are applied under periodic conditions along the tablets direction (x axis) to study the evolution of crack propagation and toughness. In order to correctly ensure this periodic condition, a thin stripe of homogenized isotropic material is added on the left-side and right-side of the numerical sample. In line with our previous work [14] and analytical models [22] a Young's modulus ratio of $\frac{E_i}{E_t} = 0.1$ is used with a Poisson's ratio of 0.21. Each sample is tested for various values of interface strength Σ_i while the tablet strength Σ_t is set to 4 GPa [12].

The imposed strain is progressively increased along the x periodic axis to propagate the crack through the numerical sample. The tensile stress and the projected crack length are used to compute the R-curve or crack extension resistance curve, i.e. the stress intensity factor versus crack length, as detailed in [14]. For each simulation, we determine the crack initiation stress intensity factor $(K_I)_{init}$ and the maximum stress intensity factor $(K_I)_{max}$ over the crack extension resistance curve [14] and calculate the difference $\Delta K_I = (K_I)_{max} - (K_I)_{init}$. The crack propagates in a very small numerical region compared to the real experiment. This means that $(K_I)_{max}$ is not representative of a typical crack growth toughness. Therefore, ΔK_I which represents the initial slope of the R-curve, is used as a measure of the toughening associated with crack propagation.

The microstructural parameters (tablet's as-

Microstructure	Mean tablet aspect ratio (ρ)	Tablet volume fraction (ϕ)	Mean tablet orientation
M0	14	0.852	90°
M1	13.48	0.849	87.2°
M2	13.62	0.852	83.4°
M3	13.60	0.851	83.1°
M4	13.52	0.850	86.8°

Table 1: Microstructural parameters issued from image analysis for the five microstructures (M0-M4).

Under notch zone	Mean tablet aspect ratio (ρ)	Tablet volume fraction (ϕ)	Mean tablet orientation
M1	13.58	0.81	86.9°
M2	13.70	0.79	85.4°
M3	13.56	0.80	78.7°
M4	13.72	0.79	86.1°

Table 2: Microstructural parameters of the region ahead of notch obtained from image analysis for the four microstructures (M1-M4).

pect ratio ρ, volume fraction ϕ and orientation along the y axis) of each image are quantified using the imageJ plugin Analysis 3D developed by [23]. The microstructure analysis of the images reveals the average values of each microstructure (Tab.1). As the mechanical response in a SENB test is suspected to be influenced by the local features near the tip of the notch, we selected a 2ax2a sized zone ahead of the notch tip (Fig.1) to compute a local value for the microstructural parameters, reported in Tab.2. In order to ensure that no bias is introduced because of truncated tablets, the total surface of the tablets intersecting the zone is considered for analysis.

Fig.2 shows a histogram of the interface thickness of the EBSD generated microstructures. It is observed that microstructure M3 has a less homogeneous distribution of the interface thickness with the presence of thick interfaces (500 nm to 700 nm) in contrast to the rest of the microstructures. Some grain growth, that might be promoted by thin or nonexistant interfaces, is also noted, especially on M3. Still, the origin of the large tablets is not totally clear as large tablets have also been noticed in the powder i.e. before

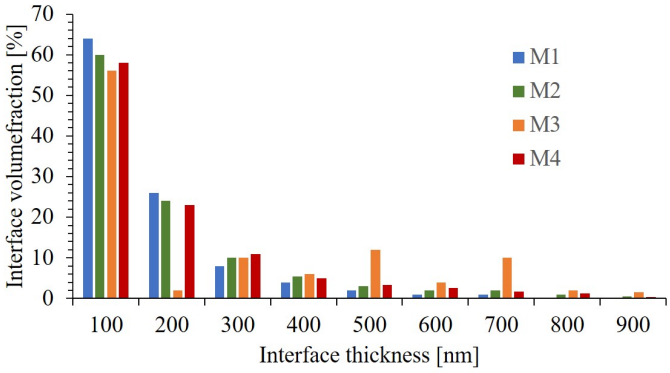

Fig. 2: Histogram of interfaces thickness for the EBSD microstructures, showing the occurrence of thicker interfaces in M3.

sintering.

Fig.3 shows an example of the stress-strain evolution before and during crack propagation of the five microstructures for an interface strength $\Sigma_i = \frac{1}{20}\Sigma_t = 200$ MPa. Stable crack propagation is observed in the EBSD-generated samples as in the regular microstructure (M0). The deflection noticed on the curve of the regular microstructure M0 that characterizes the simultaneous failure of vertical interfaces is less obvious for the other curves (i.e microstructures M1-4). It cannot be discerned in EBSD-generated microstructures as interfaces are more randomly oriented. After reaching the maximum stress, the curves become rugged, which is coherent with the pulling out of tablets observed in DEM simulations. The lowest and highest values of stress - among the EBSD-generated microstructures (M1-4)- are reached by M3 and M1, respectively.

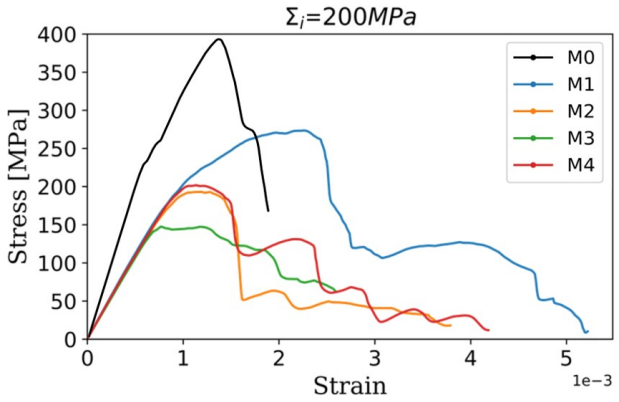

Fig. 3: An example of stress-strain curves of single edge notched samples for the five microstructures (M0-M4) with an interface strength $\Sigma_i = \frac{1}{20}\Sigma_t$=200 MPa and a fixed tablet strength of 4 GPa.

Note that regardless of the interface strength, the ranking of microstructures in terms of maximum stress remains the same (M0> M1> M4> M2> M3). In Fig. 4a the crack initiation stress intensity factor $(K_I)_{init}$ and the crack propagation toughening ΔK_I of the five samples as a function of interface strengths are compared to the regular sample (M0). Crack initiation stress intensity factor increases in a monotonic manner to reach a maximum value. The regular sample (M0) exhibits a $(K_I)_{init}$ between 20% to 36% larger than EBSD-generated microstructures.

In Fig.4b, ΔK_I increases to reach an optimum value at $\Sigma_i = \frac{1}{10}\Sigma_t$ and decreases afterwards. It is interesting to notice that the optimum value of ΔK_I is reached at the same interface strength for the regular microstructure (M0) and for the EBSD microstructures (M1-4). Similarly to crack initiation stress intensity factor, microstructures M2 and M3 exhibit lower crack propagation toughening than the other EBSD-generated microstructures. ΔK_I is 15% to 42% higher for the regular microstructure as compared to the real microstructures from EBSD. The microstructure rankings observed for $(K_I)_{init}$ and for ΔK_I are the same than for maximum stress i.e. M0> M1> M4> M2> M3.

To understand this ranking and the differences showed in Fig.3 and Fig.4, we focus on the crack propagation in microstructures M0, M1 and M3 that lead to extrema in terms of mechanical response. Fig.5 shows the crack propagation along with the stress-strain plots of microstructures for an interface strength of 200 MPa. Similar reinforcement mechanisms are noticed in the realistic and regular microstructures. First, microcracking, which is the fracture of vertical or horizontal interfaces, participates in stress relaxation at the crack tip. This mechanism helps in preserving reasonable initiation toughness even with weak interfaces. By comparing microstructures M1 and M3, it is noticeable that more damage/microcracking is present in M1 prior to crack propagation, while in M3 a smaller number of interfaces are damaged before crack propagation. This logically leads to a higher stress concentration at the crack tip in M3 and lower crack initiation stress intensity factor (Fig.4a).

Typically, when the crack starts propagating in the material through the interfaces, it gets deflected when encountering a tablet resulting in a non-straight crack pattern (M1). However, in M3, when the crack passes through the interface, it encounters two tablets with a favorable orientation for the crack propagation. This leads to a straighter pattern of the crack. In other words, if the tablet had been better aligned along the x axis direction, the crack would have deviated to-

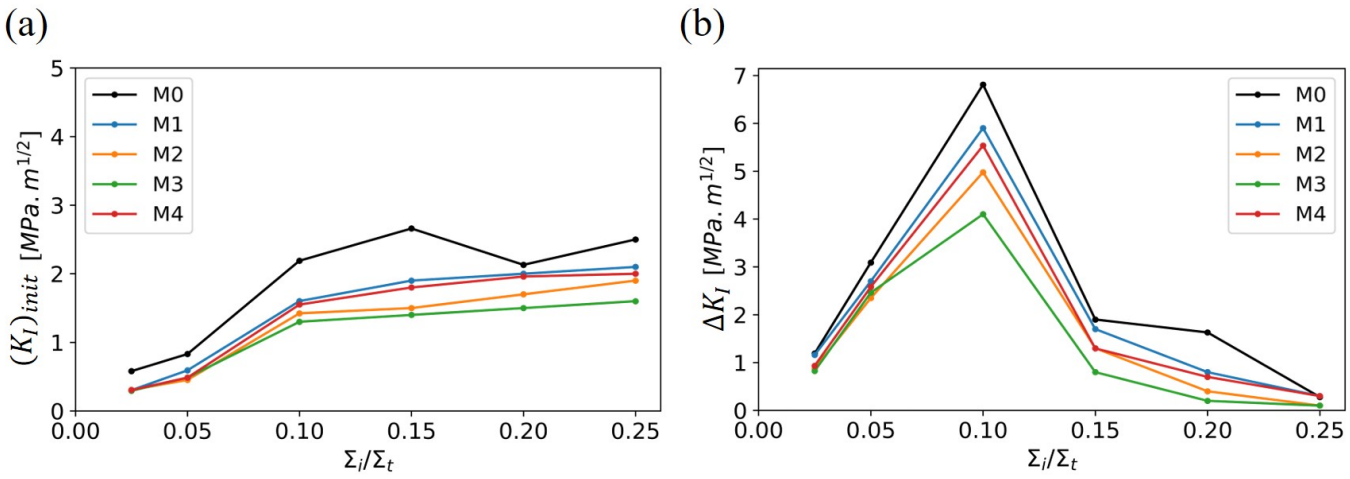

Fig. 4: a) Crack initiation stress intensity factor $(K_I)_{init}$ and b) crack propagation toughening ΔK_I of the regular microstructure (M0) and the EBSD generated microstructures (M1-4) as a function of the normalized interface strength $\frac{\Sigma_i}{\Sigma_t}$.

wards the x axis direction instead of continuing its path along the y axis direction. This contributes to the lower maximum stress (Fig.3) and crack propagation toughening (Fig.4b) reached by this microstructure.

To investigate the microstructural origins of differences in crack propagation and crack extension resistance between samples, we compare the microstructural parameters of the four microstructures. We notice that they have approximately the same tablet volume fraction, both globally (Tab. 1) and locally ahead of the crack tip (Tab. 2). However as seen in Fig 2, microstructure M3 has a less homogeneous distribution with the presence of thick interfaces (500 nm to 700 nm) in contrast to the three other microstructures. The non-homogeneous distribution of interface thickness leads to a less homogeneous distribution of the local stress which explains the lower crack extension resistance of those samples.

Tablet misorientation also plays a significant role. Indeed, as crack deviation is one of the major reinforcement mechanisms in nacre-like materials, a less deviated crack due to poorly oriented tablets results into lower crack extension resistance. Tablets in microstructure M1 have an average orientation of 87 °to the y axis, while in M3 tablets are oriented 83 °to the y axis (Tab. 1). The difference is even more marked for the local orientation ahead of the crack tip where the average orientation of M3 falls to 79 °while M1 orientation stays nearly unchanged. On the contrary, the noticeable difference in mean tablet orientation between M2 and M4 (Tab. 1) fades away locally (Tab. 2). As a consequence, M1 exhibits a better crack extension resistance than M3 while M2 and M4 have a similar behavior.

As we showed in [19], microcracking is another important reinforcement mechanism in nacre-like materials. Inspection of the crack propagation patterns in microstructure M1 indicates more microcracking compared to M3. This can be explained by the presence of thicker interfaces in M3, harder to break. The heterogeneity of interface thickness also impacts microcracking by inducing more stress localization which limits the size of the process zone. This demonstrates the possible effect of tablet orientation and interface thickness distribution on the overall behavior of this type of microstructure.

Microstructural variations play an important role in the nacre-like materials behavior. In this paper we introduced a new method to study the damage resistance of synthetic nacre-like materials by combining EBSD micrographs and DEM simulations. The simulations showed the important effect of tablet orientation and interface thickness distribution on both crack path and crack

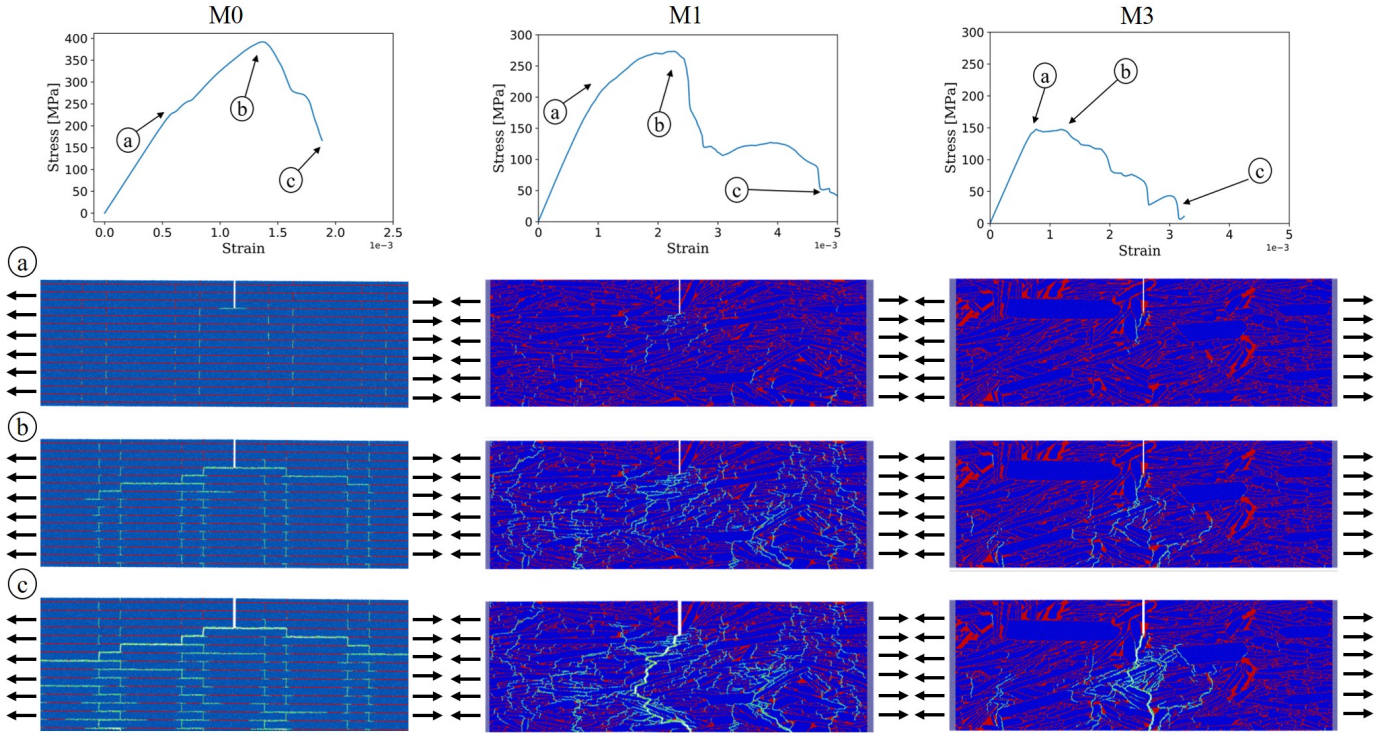

Fig. 5: Crack propagation illustrations in microstructures M0, M1 and M3 for a low interface strength (Σ_i =1/20 Σ_t= 200 MPa). Stress-strain curves and snapshots of the three main events during SENT ⓐ damage initiation, ⓑ maximum stress and ⓒ sample failure.

extension resistance. A good alignment of tablets participates in the crack deviation which leads to higher crack extension resistance. Moreover, a non-homogeneous distribution of the interface can reduce microcracking and cause the crack to follow a straight path instead of a convoluted one. The results of the simulations performed on the EBSD-generated microstructures were compared to a numerically generated regular microstructure showing a non-negligible decrease of mechanical properties for real EBSD microstructures. Even if, as shown by [18], some of disorder might be beneficial, in the case of real microstructures as investigated here, the disorder is such that more homogeneous microstructures should be sought to improve the material damage resistance. Although they provide new valuable qualitative results, a clear limitation of the discrete simulations presented here is that they apply on a much too small volume to yield unambiguous quantitative results. Thus, improvements in computing must be implemented in order to access larger volumes from images. Still, the simulations performed using EBSD microstructures can provide information unattainable by experiments and one of the short terms objectives could be the quantification of reinforcement mechanisms such as microcracking and crack deflection in order to gain knowledge on their relative importance and quantify their impact on toughness.

Acknowledgements

We acknowledge the technical support of Saint-Gobain. The Agence Nationale pour la Recherche (ANR -16- CE08-0006 BICUIT, program DS0303-2016) and the AGIR-POLE-PEM 2016 project (OMicroN) are greatly acknowledged for their financial support.

Conflict of interest

The authors declare no conflict of interest.

[1] I. Corni, T. J. Harvey, J. A. Wharton, K. R. Stokes, F. C. Walsh, and R. J. K. Wood, Bioinspiration & Biomimetics **7**, 031001 (2012).

[2] U. G. Wegst, M. Schecter, A. E. Donius, and P. M. Hunger, Philosophical Transactions of the Royal Society A: Mathematical, Physical and Engineering Sciences **368**, 2099 (2010).
[3] E. Munch, M. E. Launey, D. H. Alsem, E. Saiz, A. P. Tomsia, and R. O. Ritchie, Science **322**, 1516 (2008), arXiv:NIHMS150003 .
[4] O. Oner Ekiz, A. F. Dericioglu, and H. Kakisawa, Materials Science and Engineering C **29**, 2050 (2009).
[5] F. Bouville, E. Maire, S. Meille, A. J. Stevenson, and S. Deville, Nature Materials **13**, 1 (2014).
[6] H. Saad, K. Radi, T. Douillard, D. Jauffres, C. L. Martin, S. Meille, and S. Deville, Materialia , 100807 (2020).
[7] M. Muñoz, M. Cerbelaud, A. Videcoq, H. Saad, A. Boulle, S. Meille, S. Deville, and F. Rossignol, (2020), 10.26434/chemrxiv.12063183.v1.
[8] D. Zhu and F. Barthelat, Conference Proceedings of the Society for Experimental Mechanics Series **2**, 181 (2011).
[9] R. Yadav, R. Goud, A. Dutta, X. Wang, M. Naebe, and B. Kandasubramanian, Industrial and Engineering Chemistry Research **57**, 10832 (2018).
[10] R. K. Chintapalli, M. Mirkhalaf, A. K. Dastjerdi, and F. Barthelat, Bioinspiration & biomimetics **3** (2014).
[11] A. Doitrand, R. Henry, J. Chevalier, and S. Meille, Journal of the American Ceramic Society (2020), 10.1111/jace.17148.
[12] E. Feilden, T. Giovannini, N. Ni, C. Ferraro, E. Saiz, L. Vandeperre, and F. Giuliani, Scripta Materialia **131**, 55 (2017).
[13] H. Gao, B. Ji, I. L. Jager, E. Arzt, and P. Fratzl, Proceedings of the National Academy of Sciences **100**, 5597 (2003).
[14] K. Radi, D. Jauffres, S. Deville, and C. L. Martin, Composites Part B **183**, 107699 (2019).
[15] N. Abid, M. Mirkhalaf, and F. Barthelat, Journal of the Mechanics and Physics of Solids **112**, 385 (2018).
[16] J. William Pro, R. Kwei Lim, L. R. Petzold, M. Utz, and M. R. Begley, Journal of the Mechanics and Physics of Solids **80**, 68 (2015).
[17] A. Needleman and V. Tvergaard, International Journal of Fracture **49**, 41 (1991).
[18] N. Abid, J. W. Pro, and F. Barthelat, Journal of the Mechanics and Physics of Solids **124**, 350 (2019).
[19] K. Radi, D. Jauffrès, S. Deville, and C. L. Martin, Journal of the Mechanics and Physics of Solids **126**, 101 (2019).
[20] R. Kumar, S. Rommel, D. Jauffrès, P. Lhuissier, and C. L. Martin, International Journal of Mechanical Sciences **110**, 14 (2016).
[21] K. Radi, D. Jauffres, S. Deville, and C. L. Martin, Composites Part B , 107699 (2019).
[22] F. Barthelat, Journal of the Mechanics and Physics of Solids (2014), 10.1016/j.jmps.2014.08.008.
[23] V. Boulos, V. Fristot, D. Houzet, L. Salvo, and P. Lhuissier, in *Proceedings of the 2012 Conference on Design and Architectures for Signal and Image Processing* (2012) pp. 1–6.